

Quantum dual-path interferometry scheme for axion dark matter searches

Qiaoli Yang^{1§,*} Yu Gao^{2§,†} and Zihui Peng^{3§‡}

¹*Department of Physics and Siyuan Laboratory,
Jinan University, Guangzhou 510632, China*

²*Key Laboratory of Particle Astrophysics, Institute of High Energy Physics,
Chinese Academy of Sciences, Beijing 100049, China*

³*Key Laboratory of Low-Dimensional Quantum Structures
and Quantum Control of Ministry of Education,
Key Laboratory for Matter Microstructure and Function of Hunan Province,
Department of Physics and Synergetic Innovation
Center for Quantum Effects and Applications,
Hunan Normal University, Changsha 410081, China*

arXiv:2201.08291v4 [hep-ph] 7 Sep 2023

[§] Corresponding Authors.

Abstract

We propose a dual-path interferometry amplification configuration in cavity axion dark matter searches. We show quantum-mechanically that in a low-temperature cavity permeated by a magnetic field, the single axion-photon conversion rate is enhanced by the cavity quality factor Q and quantitatively larger than the classical result by a factor $\pi/2$. Under modern cryogenic conditions, thermal photons in the cavity are negligible; thus, the axion cavity can be considered a quantum device emitting single photons with temporal separations. This differs from the classical picture in which axions transition in batches and the converted energy accumulates in the electromagnetic field inside the cavity. It reveals a possibility for the axion cavity experiment to handle the signal sensitivity at the quantum level, e.g., cross-power and second-order correlation measurements. The correlation of photon field quadratures in the amplification chain within current technology enhances the signal-to-noise ratio compared with a single-path amplification scheme based on a high electronic mobility transistor amplifier or Josephson Parametric Amplifiers (JPAs). In particular, it is useful to combine the dual-path interferometry scheme with other techniques, e.g., JPAs, to overcome the inevitable microwave signal insertion loss (normally ~ -3 dB) in the channels between the cavity and the quantum-limited amplifiers. This enhancement would greatly reduce the signal scanning time to improve the sensitivity of the axion-photon coupling. In addition, the second-order correlation function measurement in the dual-path scheme can provide an additional verification of whether the candidate signals are axion converted or other noises.

*Electronic address: qiaoliyang@jnu.edu.cn

†Electronic address: gaoyu@ihep.ac.cn

‡Electronic address: zhihui.peng@hunnu.edu.cn

I. INTRODUCTION

The existence of cold dark matter is widely accepted [1], and one promising candidate is the axion [2–14]. The axion is a natural extension of the Standard Model of particle physics in which the amount of Charge-Parity violation by the strong interaction is determined by the vacuum angle whose value should be order one. However, experiments measuring the neutron electric dipole moment [15] suggest an essentially vanishing vacuum angle [16], thus giving rise to a puzzle known as the strong-CP problem [17, 18]. The problem could be solved by adding the Peccei-Quinn (PQ) symmetry [2, 3], which must be spontaneously broken by a PQ preserving potential and explicitly broken by the QCD instanton effect [19, 20]. The symmetry breaking implies the existence of a pseudo Nambu-Goldstone boson, which is called [14] the QCD axion, and currently, there are two QCD axion benchmark models, the KSVZ [6, 7] and the DFSZ [8, 9] models. Cosmic axions can be produced abundantly during the QCD phase transition in the early universe, and their relics compose the cold dark matter observed today [10–13]. Depending on whether the PQ symmetry occurs before or after cosmological inflation, the natural mass window of the QCD axions being the majority of dark matter is approximately $\mathcal{O}(10^{-5} - 10^{-3})\text{eV}$ [21] or $< \mathcal{O}(10^{-7})\text{ eV}$ [22], but other production mechanisms are possible, which will lead to wider mass ranges. The axion couples to the Standard Model particles weakly; in particular, it couples to two photons with a coupling $\mathcal{O}(10^{-17} - 10^{-12})\text{ GeV}^{-1}$ depending on the PQ scale. Currently, many proposed and ongoing experimental studies such as [23–30] and others are actively searching dark matter axions. Interestingly, in condensed-matter systems, quasiparticle "axions" could lead to many exciting physical phenomena [31–36] etc.. It is tempting to believe that nature has repeated itself at many different levels.

Axion haloscope experiments are based on Sikivie's resonant cavity design [37], in which the cosmic axions resonantly convert into a microwave signal in a high Q cavity permeated by a magnetic field. Although the axion-photon coupling is small, the conversion rate is enhanced by the coherence of the axion field, the magnitude of the magnetic field, and the high Q of the cavity. Modern cryogenic technology can sustain $\mathcal{O}(20)\text{ mK}$ or lower temperature, which results in a subunity thermal photon occupation number $\bar{n} \sim 10^{-5}$ at the resonant frequency (typically at several GHz) in the cavity. Therefore, it is useful to consider the quantum transition picture in the cavity, especially at such a low photon

occupation number. We find that the Q factor enhances the axion-photon transition at the quantum level which could be used to facilitate dark matter axion searches.

In this paper, we propose using a 50/50 beam splitter followed by linear amplifiers or detectors to construct a dual-path measurement scheme that realizes Hanbury Brown and Twiss (HBT) interferometry [38] in quantum optics. Linear detectors (phase-preserving amplifiers) are widely used in axion haloscope experiments. Current commercial cryogenic high electron mobility transistors (HEMT) [39] already offer a flat gain over a frequency range of 10 GHz with the addition of random noise at 10-20 photons [39], and amplifiers such as the Josephson Parametric Amplifier (JPA) [40] can approach the standard quantum limit (SQL). At very low signal/thermal photon occupation numbers, the major sensitivity hurdles are due to quantum fluctuations and added noise in the detection channel. The general method of signal identification is to accumulate sufficient statistics at each given frequency point, so it takes a very long integration time due to the unfavorable signal-to-noise ratio. The interferometer scheme in microwave quantum optics, however, has already been demonstrated to achieve *high* noise reduction [41–44], as the uncorrelated noises in the dual receiver chains cancel and the correlations of field quadratures can be measured. With this scheme, the effective correlated noise level can be significantly lower than the noise level in a single amplification channel because the interferometer scheme is not sensitive to the inevitable microwave signal insertion loss in the channels between the cavity and the amplifiers.

II. AXION CAVITY AT THE QUANTUM LEVEL

The QCD axion was proposed to solve the strong CP problem. Its couplings to the standard model particles cannot be arbitrarily weak; otherwise, the axions would be over-produced in the early universe. Nevertheless, the viable “invisible axion” models give rise to extremely weak couplings and very light masses that hinder axion experimental searches. Fortunately, the dark matter axion production mechanism [10–13] hints at a preferred axion mass window around neV, although the uncertainty could be several orders of magnitude. Various dark matter axion search methods aimed at this mass window have been proposed. In these proposals, the axion cavity haloscopes are particularly sensitive and are the only experiments that can reach the QCD axion parameter space to date. The original calcula-

tion was given [37, 45] in a picture in which the cavity captures the photons produced and enhances the conversion process through resonance when one of the cavity modes matches the energy of the axion signal. However, it was uncertain whether the transition rate can be enhanced during a single axion-photon conversion, which is quantum in nature. Some calculations, e.g., Ref. [46], applied the Feynman diagram method, which requires the existence of asymptotic outgoing states and thus cannot derive the resonant cavity's enhancement and form factor.

The axion field a couples to the photons by

$$\mathcal{L}_{a\gamma\gamma} = -g_{a\gamma\gamma} a \vec{E} \cdot \vec{B} \quad , \quad (1)$$

where the axion-photon coupling $g_{a\gamma\gamma}$ is defined as $g_{a\gamma\gamma} = c_\gamma \alpha / (\pi f_a)$, f_a is the PQ scale factor, $\alpha = 1/137$ is the fine-structure constant and c_γ is a model-dependent factor order of one.

The present-day axion dark matter halo profile is crucial to axion searches, but luckily, there are only two important factors for the current discussion: (i) the dark matter halo has a local density $\rho_a = \rho_{CDM} \approx 0.45 \text{ GeV}/\text{cm}^3$; (ii) the axion dark matter is highly coherent, which is a consequence of the small axion mass m_a and its slow velocity $v_a \sim 10^{-3}c$ in the halo.

Due to the small axion mass and the low velocity, the axion dark matter has a long de-Broglie wavelength $\lambda_a = 2\pi/(m_a v) \sim \mathcal{O}(1 - 100)$ meters, much larger than the size of a respective resonant cavity so the axion field is homogeneous in a haloscope cavity. In addition, the axion coherence time $\tau_a = \lambda_a/\delta v_a \sim 2\pi/(m_a v_a^2)$ is also significantly longer than the photon existence time in the cavity: $\tau_c = 2\pi Q/\omega_a \approx 2\pi Q/m_a$, where $Q \sim 10^5$ for current state-of-the-art technology; thus, the axion field can be regarded as monochromatic during a cavity model transition (note that in some axion halo models, the coherence time could be even longer if $\delta v_a \ll v_a$ [47, 48]). Thus, we can write the axion field as

$$a \approx a_0 \cos(\omega_a t) = \frac{\sqrt{2\rho_a}}{m_a} \cos(\omega_a t) \quad . \quad (2)$$

In the experimental literature, the axion quality factor $Q_a = 1/v_a^2 \sim 10^6$ is often used to describe the coherence of axions.

In a cavity, the electric field operator \vec{E} can be expanded as

$$\vec{E} = i \sum \sqrt{\frac{\omega_k}{2}} [a_k \vec{U}_k(\vec{r}) e^{-i\omega_k t} - a_k^\dagger \vec{U}_k^*(\vec{r}) e^{i\omega_k t}] \quad , \quad (3)$$

where a_k , and a_k^\dagger are the annihilation and creation operators for the photon Fock state, respectively, $\vec{U}_k(\vec{r})$ is the cavity mode satisfying the wave equation $(\nabla^2 + \omega_k^2)\vec{U}_k(\vec{r}) = 0$ with cavity-wall boundary conditions, and k denotes different cavity modes. Assuming that the permitted magnetic field is along the \hat{z} direction, $\vec{B} = \hat{z}B_0$, the interaction Hamiltonian can be written as

$$\begin{aligned} H_I &= - \int d^3x \mathcal{L}_{a\gamma\gamma} \\ &= \left(g_{a\gamma\gamma} \frac{\sqrt{2\rho_a}}{m_a} B_0 \int d^3x \hat{z} \cdot \vec{E} \right) \cos(\omega_a t) . \end{aligned} \quad (4)$$

Up to the first order, the photon $|0\rangle \rightarrow |1\rangle$ transition probability is

$$\begin{aligned} P &\approx \left| \langle 1 | \int_0^t dt H_I | 0 \rangle \right|^2 \\ &\approx g_{a\gamma\gamma}^2 \frac{\rho_a}{m_a^2} B_0^2 \sum_k \omega_k \left| \int d^3x \hat{z} \cdot \vec{U}_k^* \right|^2 \\ &\times \frac{\sin^2[(\omega_k - \omega_a)t/2]}{4[(\omega_k - \omega_a)/2]^2} . \end{aligned} \quad (5)$$

When t is large, we can use the approximation $\sin^2(\Delta\omega t/2)/[\Delta\omega/2]^2 \approx 2\pi t \delta(\Delta\omega)$. The transition rate is $R = dP/dt$. Let us define the form factor

$$C_k = \frac{\left| \int d^3x \hat{z} \cdot \vec{U}_k \right|^2}{V \int d^3x |\vec{U}_k|^2} , \quad (6)$$

where V is the volume of the cavity, and the factor $\int d^3x |\vec{U}_k|^2$ properly normalizes the photon field operator. Then we have

$$R \approx \frac{\pi}{2} g_{a\gamma\gamma}^2 \frac{\rho_a}{m_a^2} B_0^2 V \sum_k C_k \omega_k \delta(\omega_k - \omega_a) . \quad (7)$$

Since $\sum_k C_k \omega_k \delta(\omega_k - \omega_a) \approx \int C_k d\omega (\omega/d\omega) \delta(\omega - \omega_a) \approx Q C_{\omega_a}$, we have the transition rate

$$R \approx \frac{\pi}{2} g_{a\gamma\gamma}^2 \frac{\rho_a}{m_a^2} B_0^2 C_{\omega_a} V Q . \quad (8)$$

This shows that the single axion-photon transition power $P_{sig} = \omega_a R \approx m_a R$ is *enhanced* by the cavity's quality factor Q , which is in good agreement with the calculation in the classical picture. For a typical haloscope setup, the cavity volume is approximately one liter, with $Q \sim 10^5$ and $B \sim 10$ T magnetic fields, and the $a \rightarrow \gamma$ conversion rate is approximately

$\mathcal{O}(1)$ per second for the QCD axions; thus, the signal temporal separations far exceed the resolution of linear detectors.

The thermal photon occupation number in the cavity is

$$n(\omega_a, T) = \frac{1}{e^{\omega_a/k_B T} - 1} . \quad (9)$$

For axion mass $m_a \geq 10^{-5}\text{eV}$ and a cavity operating at approximately $T \approx 20$ mK, the thermal photon state has a low occupation number $n \ll 1$; thus, the cavity is almost always in the vacuum state. It is convenient to define the cavity coupling parameter $\beta = Q_0/Q_c$, where Q_0 is the quality factor due to the photon losses by cavity-wall absorption and Q_c is due to the photons leaving the cavity. The combined quality factor is then $Q^{-1} = Q_0^{-1} + Q_c^{-1}$, and the photon emission rate is $R \cdot \beta/(1 + \beta)$. Ideally, $\beta \sim 1$ is the optimal working point, but its exact value depends on the cavity design. In summary, the axion cavity can be regarded as a single photon emitter with a slow rate of $R \lesssim 10$ Hz.

III. DUAL-PATH INTERFEROMETRY

Since the axion cavity is a single-photon emitter at low pulse rates, the major experimental bottleneck lies in the detection sensitivity to weak microwave signals at the single-photon level. To date, practical microwave single-photon detectors have yet to be realized, mainly because the microwave photon energy is several orders of magnitude lower than that of an optical photon, resulting in the detection difficulty of microwave single photons [49]. Currently, a typical linear detector scheme for an axion cavity search consists of an amplification chain, which is a cryogenic HEMT amplifier as a preamplifier placed at the 4 K temperature stage in a dilution refrigerator, and subsequent room-temperature amplifiers. The amplified microwave signal at GHz was downconverted to a few tens of MHz and then sampled by digitizers at room temperature. The typical noise temperature of a cryogenic HEMT is approximately several Kelvin. Considering the loss in the channel from the microwave signal emitted from the cavity at the 20 mK stage to the cryogenic HEMT placed at the 4 K stage in the refrigerator, the effective noise temperature T_{eff} in the detection channel could be higher than 10 K. With the development of superconducting quantum information technology, recent axion cavity experiments, such as ADMX-Sidecar [50], QUAX- $a\gamma$ [51], etc., have applied JPAs as a preamplifier to enhance detection sensitivity. However, there is

possible deterioration of the superconducting JPA in a strong magnetic field environment, and there is approximately ~ -3 dB insertion loss from coaxial cables, switchers and circulators placed between the cavity and the quantum-limited amplifiers T_{eff} of the detection channel, which is approximately four times higher than the SQL [50].

Thus, the effective temperature T_{eff} on readout is often much higher than the physical temperature in the cavity. The signal-to-noise ratio is

$$\text{SNR} = \frac{P_{sig}}{k_B T_{eff}} \sqrt{\frac{t}{b}} , \quad (10)$$

where b is the detection bandwidth, P_{sig} is the signal power, k_B is the Boltzmann constant and t is the integration time. The sensitivity on $g_{a\gamma}^2$ is inversely proportional to T_{eff} or grows over the square root of the integrated time.

Here, we briefly interpret the quantum noise with detector observables,

$$\hat{I}_r \cos(\omega_a t) + \hat{Q}_r \sin(\omega_a t) = \text{Re} \left((\hat{I}_r + i\hat{Q}_r) e^{i\omega_a t} \right) \quad (11)$$

where we define the in-phase \hat{I}_r and quadrature \hat{Q}_r component operators with $\hat{I}_r = (\hat{r}^\dagger + \hat{r})/2$, $\hat{Q}_r = -i(\hat{r}^\dagger - \hat{r})/2$ using the creation and annihilation operators \hat{r}^\dagger and \hat{r} . These operators satisfy commutation relations

$$[\hat{I}_r, \hat{Q}_r] = i/2 \quad \text{and} \quad [\hat{r}^\dagger, \hat{r}] = 1 . \quad (12)$$

Assuming the linear detector enhances the field by a gain of G , we have

$$\frac{\hbar\omega_a}{2} + \frac{(G^2 - 1)\hbar\omega_a}{2G^2} \approx \hbar\omega_a, \quad (13)$$

and for a large G , this is often called the SQL [52]. To protect the cavity at 20 mK from thermal noise leakage from the second-stage amplifier (e.g., cryogenic HEMT at 4 K), preamplifier gain over 20 dB is needed. To the best of our knowledge, it is still difficult to achieve 20 dB gain over a 1 GHz bandwidth for a JPA or a traveling-wave parametric amplifier (TWPA) [53], with the noise level approaching the SQL simultaneously.

For signals with quantum origin, a dual-path measurement can be a powerful tool because it measures the statistical correlation between quadratures in the two channels in addition to the photon number $n = \langle a^\dagger a \rangle$ in each channel. Recent quantum optics developments enable dual-path detection in the microwave-frequency domain, and it can be performed with phase-preserving linear amplifiers as well [41–44, 54]. Linear amplifiers are well known

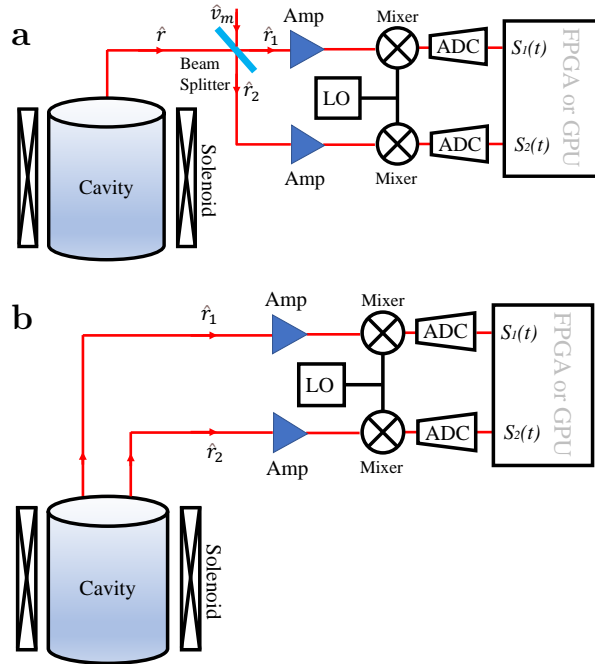


FIG. 1: Scheme of the quantum dual-path setup for a resonant cavity dark matter axion search. (a) Single-sided cavity scheme. There is only one output port of the cavity detector. Axions convert to microwave single photons that escape from the cavity as a propagation quantum field with an annihilation operator \hat{r} and subsequently pass through a 50/50 beam splitter along with a vacuum field or weak thermal field \hat{v}_m near the cavity at the 20 mK stage in a refrigerator. The output fields \hat{r}_1 and \hat{r}_2 are then amplified by two nominally identical amplification chains (denoted as AMP) and downconverted into intermediate (e.g., 25 MHz) frequency ω_{if} with a mixer by the local oscillator (LO) at the same frequency as the cavity's resonance frequency. The field quadratures are recorded by analog-to-digital converters (ADCs), and the complex envelopes S_i are then extracted and calculated by FPGA or GPU electronics in real time. The single-sided cavity scheme can overcome the inevitable insertion loss between the beam splitter and the AMP. (b) Two-sided cavity scheme. If there are two identical output ports of the cavity detector, the converted microwave single photons escape from the two output ports with equal probability, and a beam splitter is not necessary. The correlations between the two cavity outputs behave similarly to the outputs of the beam splitter in (a). However, it is expected that the SNR in this scheme is even higher than that in the scheme described in (a). It can overcome the inevitable insertion loss between the cavity and the AMP.

for their high signal gain for weak electromagnetic field signals but at the cost of extra noise. With a 50/50 beam splitter, as shown in Fig. 1, dual linear amplifier chains can be constructed to measure the signal correlation information. It has been shown [41, 42, 44] that with a recording of the full time traces of the signals in both channels instead of the time-averaged value in a single channel, the signal's cross power in two channels can be extracted and significantly improves the SNR.

The dual-path scheme in Fig. 1(a) forms a Hanbury Brown-Twiss interferometer setup. The axion cavity acts as a quantum emitter to inject a microwave single-photon field \hat{r} , which passes through a microwave-frequency beam splitter. The beam splitter gives rise to two output fields in channels 1 and 2,

$$\hat{r}_1 = (\hat{r} + \hat{\nu}_m)/\sqrt{2} \quad \text{and} \quad \hat{r}_2 = (\hat{r} - \hat{\nu}_m)/\sqrt{2} \quad . \quad (14)$$

$\hat{\nu}_m$ is the added noise field, for instance, $\hat{\nu}_m$ as the vacuum state or a weak thermal state. Then, by measuring $\hat{I}_1 = (\hat{r}_1 + \hat{r}_1^+)/2$ and $\hat{Q}_2 = -i(\hat{r}_2 - \hat{r}_2^+)/2$, a complex observable can be constructed as

$$\hat{S}_a(t) = I_1(t) + iQ_2(t) = \hat{r} + \hat{\nu}_m^+ \quad . \quad (15)$$

In fact, $\hat{S}_a(t)$ behaves classically and resembles a complex number because $\hat{S}_a^+ = \hat{S}_a^*$ and $[\hat{S}_a^+, \hat{S}_a] = 0$ under the effect of the added noise ν_m [55]. After amplification and mixing, the two classical complex envelopes $S_i(t)$, $i = 1, 2$, at the digitizers can be written as

$$S_i(t) = G_i \hat{r}(t) + \sqrt{G_i^2 - 1} h_i^+(t) + \nu_{m,i}^+(t) \quad , \quad (16)$$

where we let h_i denote the added thermal noise in each linear amplifier chain and $\nu_{m,i}(t)$ denote the vacuum noise. Both quadratures of \hat{S}_i can be measured simultaneously by digitizers due to the commutator $[\hat{S}_i, \hat{S}_i^+] = 0$. A powerful Field Programmable Gate Array (FPGA) [41, 42] or Graphics Processing Unit (GPU) [44] can analyze the correlation of field quadratures in real time. The correlations of the output field quadratures are constructed as

$$\langle (S_i^*)^m S_j^n \rangle = \langle (S_i^+)^m S_j^n \rangle = \langle (\hat{r}^+)^m \hat{r}^n \rangle \quad , \quad (17)$$

with integer-number power indexes m and n .

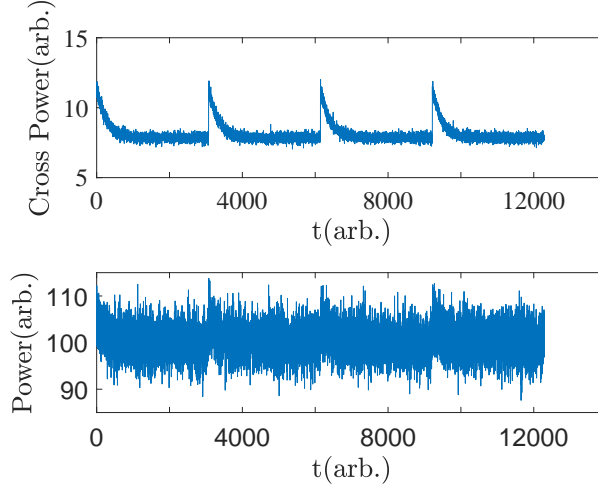


FIG. 2: Illustrative comparison between simulated cross power (upper) and single-channel power (lower). A periodical signal is injected with white noise. The signal-to-noise ratio is much higher when using the cross-power setup that reveals the injected signal.

IV. SENSITIVITY ENHANCEMENT

It is now straightforward to show that the signal can be picked up by the instantaneous power function $\langle S_i^*(t)S_j(t) \rangle$, where the *power* is

$$\langle S_i^*(t)S_i(t) \rangle = G_i^2 (\langle \hat{r}^+(t)\hat{r}(t) \rangle + N_i + 0.5) \quad , \quad (18)$$

and the *cross-power* is

$$\langle S_1^*(t)S_2(t) \rangle = G_1G_2 (\langle \hat{r}^+(t)\hat{r}(t) \rangle + N_{12} + 0.5) \quad , \quad (19)$$

respectively. Here, the component $P_{\text{cavity}} = \langle \hat{r}^+(t)\hat{r}(t) \rangle$ identifies the power from the cavity, $N_i = (G_i^2 - 1) \langle h_i^+ h_i \rangle / G_i^2$ is the power of noise added in a single channel, and $N_{12} = \sqrt{(G_1^2 - 1)(G_2^2 - 1)} \langle h_1 h_2^+ \rangle / G_1G_2$ is the power of correlated noise between channels 1 and 2. $\langle h_1 h_2^+ \rangle \sim 0$ because the two noise modes in the two detection channels are commutable and mostly uncorrelated. That is,

$$N_{12} + 0.5 \ll N_i + 0.5 \quad , \quad (20)$$

and the magnitude of dual-path noise is significantly lower than the magnitude of single-path noise, as illustrated in Fig 2. Notably, $N_{12} + 0.5 \geq 0.5$ and $N_i + 0.5 \geq 1$ are related to the noise set by SQL. The SNR in the dual-path scheme is enhanced two times compared

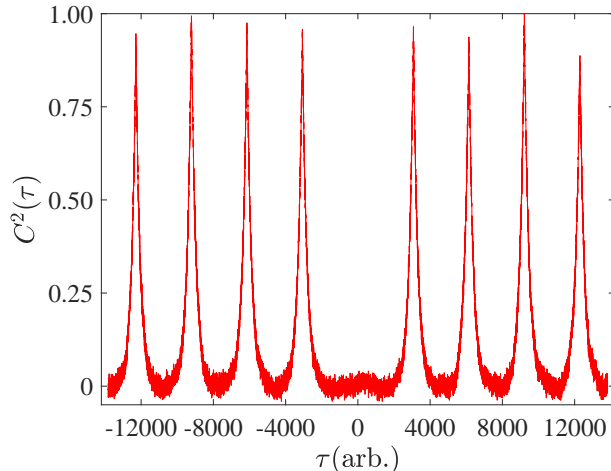


FIG. 3: Simulation of the second-order correlation function measurement for a single-photon pulse train with white noise. If photon antibunching is observed in the experiment as $C^2(0) < C^2(\tau)$, the converted periodic signal is nonclassical.

to that in the single-path scheme only in the ideal case. We emphasize that it is crucial to upgrade from the traditional single-path setup to *dual-path* to cancel the main part of uncorrelated noises from different detection channels in real experiments. In practice, N_i is almost larger than 4 because of the possible deterioration of the superconducting JPA in a strong magnetic field environment and the microwave signal insertion loss between the cavity and the detector in the current single-path experiment with JPAs working in the GHz frequency range [50]. If the search frequency range is lower than 1 GHz, N_i is even larger than 10 in the real experiment [30]. However, the scale of the remaining correlated noise N_{12} depends on the experimental devices and can be suppressed to much smaller than 0.5, and it can be directly measured by the cross power without an axion cavity. This can be explained by the thermal leakage from the cryogenic HEMT at 4 K inducing correlated noise between the two channels of the beam splitter. Actually, it has been demonstrated that the correlated noise N_{12} can be reduced and the SNR of the dual-path scheme can be enhanced for the cross-power measurement if there are quantum isolators or JPAs between the beam splitter and HEMT at 4 K [54].

The preamplifiers or detectors can be placed at a distance from the cavity output port to help shield the strong magnetic field. Insertion loss is inevitable because there are a series of microwave coaxial cables, switches and circulators between the cavity port and the pream-

plifiers/detectors. In realistic experiments, for instance, the effective noise temperature in the detection channel is ~ 925 mK at 4.798 GHz even when using JPA with an insertion loss ~ -3 dB [50]. However, the effective noise temperature should be ~ 240 mK if it is only limited by the SQL. Therefore, there is an obvious advantage to using a dual-path interferometer scheme that can approach the effective noise temperature with ~ 120 mK, which comes from quantum vacuum fluctuations, especially to use the two-sided cavity scheme described in Fig.1(b) to detect converted microwave single-photon signals. In the two-sided cavity dual-path scheme, there are two identical output ports, and the converted microwave single photons escape from them with equal probability. The correlations between the two cavity outputs behave similarly to the outputs of the beam splitter in Fig. 1(a). The dual-path interferometer is not sensitive to loss or thermal noise in the single channel, and the SNR could be enhanced by one order of magnitude compared with the single-path amplification scheme based on JPA.

Recent dual-path setups [41–44] showed that by using cross-power, the effective noise temperature could be reduced compared to that of a single channel. Fig. 2 illustrates the noise level reduction with the simulation of cross-power between two channels and the power in one channel averaged over the same time. It has been demonstrated that in a dual-path experiment with a cryogenic HEMT as preamplifiers, the correlated noise temperature is approximately 80 mK and the effective total noise temperature is approximately 180 mK, corresponding to half microwave photon noise, for the signal at 7.2506 GHz in the dual-path setup, which is much smaller than the characteristic ~ 10 K noise in each detection chain [42].

By Eq. 10, the SNR with a cross-power measurement is much higher than the power calculation by replacing the SQL with a reduced effective noise temperature. This allows faster signal-significance accumulation and reduces the amount of required time-exposure at each frequency point in future cavity axion dark matter search, esp. at relatively high frequencies. Actually, the assumption of equal gain in both amplification channels and a balanced microwave beam splitter is not difficult to achieve in experiments [41–44], and even an unbalanced detection channel does not hinder the cancellation of correlated noise.

V. THE SECOND-ORDER CORRELATION FUNCTION MEASUREMENT

Interestingly, for power correlation statistics, one may consider

$$\begin{aligned} C^2(t, t + \tau) &= \langle \hat{r}^+(t) \hat{r}^+(t + \tau) \hat{r}(t + \tau) \hat{r}(t) \rangle \\ &= 4 \langle S_1^+(t) S_1^+(t + \tau) S_2(t + \tau) S_2(t) \rangle. \end{aligned} \quad (21)$$

As widely exploited in quantum optics, single-photon signals demonstrate two important features: sub-Poissonian statistics $C^2(\tau) \leq 1$ and photon anti-bunching $C^2(0) < C^2(\tau)$ [42–44, 54]. When a signal candidate emerges during a scan, the second-order function measurement, as simulated in Fig. 3, allows the measured $C^2(0)$ value to verify the nature of the signal: whether it is converted as a single photon from dark matter axion ($C^2(0) \sim 0$) or simply from thermal noise ($C^2(0) \sim 1$). ($C^2(0) \sim 0$) arises from the fact that a single photon can only arrive at one path at one time, and it is a well-known technique in quantum optics to veto thermal noise [41–44]. Thus, our dual-path scheme can provide an additional test of the signal’s nature when the cavity’s predicted occupation numbers are small, in which case most axion-converted signals exit the cavity as single photons.

We must emphasize that it is easy to combine the quantum dual-path scheme with other techniques, such as JPAs, microwave squeezing-state, and single-photon detectors. Even with JPAs, the single-path noise temperature is approximately four times higher than that limited by the SQL [50]. However, with the dual-path measurement setup, noise due to the SQL in a single path could be avoided. With the squeezing state, a fractional breaching of SQL has been achieved [56], while for cross-power, at least an order of magnitude difference between correlated and uncorrelated noise levels is typically expected [41–44]. In addition, both JPA and squeezing-state techniques have rather small working bandwidths compared to that of cryogenics HEMT. It is also expected that the effective noise temperature can be further lowered by using JPA or TWPA as preamplifiers to protect the axion haloscope detector and beam splitter from thermal noise leaked from the high temperature stage, e.g., HEMT at 4 K [54]. It was proposed to detect the axion by a microwave single-photon detector [57]. We emphasize that it is also easy to combine the dual-path measurement setup with a single-photon detector, and it is expected that the SNR of axion detection reaches a limit from the temperature of the axion haloscope cavity itself. We think the best way would be to combine a dual-path scheme with broad-band, high-efficiency single-photon

detectors for application in axion search in the future.

VI. SUMMARY

The axion cavity signal can be modeled quantum-mechanically at a low transition rate as a single photon Fock state in the cavity is populated and then quickly decayed. We show that the single-photon $a \rightarrow \gamma$ transition rate is amplified by the cavity Q -factor, consistent with the classical picture. Since the axion cavity acts as a quantum signal emitter, it is very effective to employ the cross-power measurement in a dual-path interferometry setup instead of using a single channel receiver. The single-photon signal is slitted by a 50/50 beam splitter and then amplified and mixed by heterodyne detectors. With a digital analyzer, the measured cross-power effectively reduces the noise level due to the cancellation of uncorrelated noise in the two channels. Compared to the traditional single-channel readout, a high enhancement in the signal-to-noise ratio can be achieved with the current dual-path setup with the HEMT as the preamplifiers and a higher enhancement for the JPA as the preamplifiers because the amplified vacuum variance (the minimum is 0.5 photons) is avoided. Thus, combining the dual-path interferometry scheme with other techniques, e.g., single-photon detectors, could approach the noise temperature limited by the temperature of the axion haloscope cavity itself. The dual-path scheme can provide a substantially faster scanning rate for axion dark matter searches or, equivalently, a much higher sensitivity of axion photon coupling. The second-order correlation function measurement can provide a test of the single-photon nature of an axion-conversion signal.

Acknowledgments

The authors thank Pierre Sikvie, Giovanni Carugno, Lan Zhou, Yu-Xi Liu and Chang-Ling Zou for helpful discussions. Q.Y. is supported by NSFC under Grant No. 11875148 and No. 12150010. Y.G. is supported by NSFC under Grant No. 12150010 and is partially supported by the National R&D Program of China, 2020YFC2201601. Z.P. is supported by

NSFC under Grant Nos. 61833010, 12074117, and 12061131011.

- [1] P. A. R. Ade et al. (Planck), *Astron. Astrophys.* **594**, A13 (2016), 1502.01589.
- [2] R. D. Peccei and H. R. Quinn, *Phys. Rev. Lett.* **38**, 1440 (1977), [[328\(1977\)](#)].
- [3] R. D. Peccei and H. R. Quinn, *Phys. Rev.* **D16**, 1791 (1977).
- [4] S. Weinberg, *Phys. Rev. Lett.* **40**, 223 (1978).
- [5] F. Wilczek, *Phys. Rev. Lett.* **40**, 279 (1978).
- [6] J. E. Kim, *Phys. Rev. Lett.* **43**, 103 (1979).
- [7] M. A. Shifman, A. I. Vainshtein, and V. I. Zakharov, *Nucl. Phys.* **B166**, 493 (1980).
- [8] A. R. Zhitnitsky, *Sov. J. Nucl. Phys.* **31**, 260 (1980), [[Yad. Fiz.31,497\(1980\)](#)].
- [9] M. Dine, W. Fischler, and M. Srednicki, *Phys. Lett.* **104B**, 199 (1981).
- [10] J. Preskill, M. B. Wise, and F. Wilczek, *Phys. Lett.* **B120**, 127 (1983), [[URL\(1982\)](#)].
- [11] L. F. Abbott and P. Sikivie, *Phys. Lett.* **B120**, 133 (1983), [[URL\(1982\)](#)].
- [12] M. Dine and W. Fischler, *Phys. Lett.* **B120**, 137 (1983), [[URL\(1982\)](#)].
- [13] P. Sikivie, *Phys. Rev. Lett.* **48**, 1156 (1982).
- [14] F. Wilczek (1991).
- [15] R. J. Crewther, P. Di Vecchia, G. Veneziano, and E. Witten, *Phys. Lett. B* **88**, 123 (1979),
[Erratum: *Phys.Lett.B* 91, 487 (1980)].
- [16] C. A. Baker et al., *Phys. Rev. Lett.* **97**, 131801 (2006), [hep-ex/0602020](#).
- [17] R. D. Peccei, *Lect. Notes Phys.* **741**, 3 (2008), [hep-ph/0607268](#).
- [18] J. E. Kim and G. Carosi, *Rev. Mod. Phys.* **82**, 557 (2010), [Erratum: *Rev.Mod.Phys.* 91,
049902 (2019)], [0807.3125](#).
- [19] C. G. Callan, Jr., R. F. Dashen, and D. J. Gross, *Phys. Rev. D* **17**, 2717 (1978).
- [20] C. Vafa and E. Witten, *Phys. Rev. Lett.* **53**, 535 (1984).
- [21] P. Sikivie, *Lect. Notes Phys.* **741**, 19 (2008), [astro-ph/0610440](#).
- [22] M. P. Hertzberg, M. Tegmark, and F. Wilczek, *Phys. Rev. D* **78**, 083507 (2008), [0807.1726](#).
- [23] S. De Panfilis, A. C. Melissinos, B. E. Moskowitz, J. T. Rogers, Y. K. Semertzidis, W. Wuensch,
H. J. Halama, A. G. Prodell, W. B. Fowler, and F. A. Nezrick, *Phys. Rev. Lett.* **59**, 839 (1987).
- [24] C. Hagmann, P. Sikivie, N. S. Sullivan, and D. B. Tanner, *Phys. Rev. D* **42**, 1297 (1990).
- [25] Y. Kahn, B. R. Safdi, and J. Thaler, *Phys. Rev. Lett.* **117**, 141801 (2016), [1602.01086](#).

- [26] A. Caldwell, G. Dvali, B. Majorovits, A. Millar, G. Raffelt, J. Redondo, O. Reimann, F. Simon, and F. Steffen (MADMAX Working Group), *Phys. Rev. Lett.* **118**, 091801 (2017), 1611.05865.
- [27] L. Zhong et al. (HAYSTAC), *Phys. Rev. D* **97**, 092001 (2018), 1803.03690.
- [28] D. J. E. Marsh, K.-C. Fong, E. W. Lentz, L. Smejkal, and M. N. Ali, *Phys. Rev. Lett.* **123**, 121601 (2019), 1807.08810.
- [29] J. Schütte-Engel, D. J. E. Marsh, A. J. Millar, A. Sekine, F. Chadha-Day, S. Hoof, M. N. Ali, K.-C. Fong, E. Hardy, and L. Šmejkal, *JCAP* **08**, 066 (2021), 2102.05366.
- [30] C. Bartram et al. (ADMX), *Phys. Rev. Lett.* **127**, 261803 (2021), 2110.06096.
- [31] F. Wilczek, *Phys. Rev. Lett.* **58**, 1799 (1987).
- [32] A. M. Essin, J. E. Moore, and D. Vanderbilt, *Phys. Rev. Lett.* **102**, 146805 (2009), 0810.2998.
- [33] R. Li, J. Wang, X. Qi, and S.-C. Zhang, *Nature Phys.* **6**, 284 (2010), 0908.1537.
- [34] D. Xiao et al., *Phys. Rev. Lett.* **120**, 056801 (2018), 1710.00471.
- [35] A. Bermudez, L. Mazza, M. Rizzi, N. Goldman, M. Lewenstein, and M. A. Martin-Delgado, *Phys. Rev. Lett.* **105**, 190404 (2010), URL <https://link.aps.org/doi/10.1103/PhysRevLett.105.190404>.
- [36] D. M. Nenko, C. A. C. Garcia, J. Gooth, C. Felser, and P. Narang, *Nature Rev. Phys.* **2**, 682 (2020).
- [37] P. Sikivie, *Phys. Rev. Lett.* **51**, 1415 (1983), [Erratum: *Phys.Rev.Lett.* 52, 695 (1984)].
- [38] R. H. Brown and R. Q. Twiss, *Nature* **177**, 27 (1956).
- [39] URL <https://www.lownoisefactory.com/products/>.
- [40] M. Hatridge, R. Vijay, D. H. Slichter, J. Clarke, and I. Siddiqi, *Physical Review B* **83** (2011), ISSN 1550-235X, URL <http://dx.doi.org/10.1103/PhysRevB.83.134501>.
- [41] E. P. Menzel, F. Deppe, M. Mariani, M. Araque Caballero, A. Baust, T. Niemczyk, E. Hoffmann, A. Marx, E. Solano, and R. Gross, *Physical Review Letters* **105** (2010), ISSN 1079-7114, URL <http://dx.doi.org/10.1103/PhysRevLett.105.100401>.
- [42] D. Bozyigit, C. Lang, L. Steffen, J. Fink, C. Eichler, M. Baur, R. Bianchetti, P. Leek, S. Filipp, M. da Silva, et al., *Nature Phys* **7**, 154 (2011).
- [43] Z. H. Peng, S. E. de Graaf, J. S. Tsai, and O. V. Astafiev, *Nature Communications* **7** (2016), ISSN 2041-1723, URL <http://dx.doi.org/10.1038/ncomms12588>.
- [44] Y. Zhou, Z. Peng, Y. Horiuchi, O. Astafiev, and J. Tsai, *Physical Review Applied* **13** (2020), ISSN 2331-7019, URL <http://dx.doi.org/10.1103/PhysRevApplied.13.034007>.

- [45] P. Sikivie, Phys. Rev. D **32**, 2988 (1985), [Erratum: Phys.Rev.D 36, 974 (1987)].
- [46] M. Beutler, A. Pargner, T. Schwetz, and E. Todarello, JCAP **02**, 026 (2019), 1812.05487.
- [47] P. Sikivie, Phys. Lett. B **567**, 1 (2003), astro-ph/0109296.
- [48] C. Armendariz-Picon and J. T. Neelakanta, JCAP **03**, 049 (2014), 1309.6971.
- [49] A. Blais, A. L. Grimsmo, S. M. Girvin, and A. Wallraff, Rev. Mod. Phys. **93**, 025005 (2021), 2005.12667.
- [50] C. Bartram et al. (2021), 2110.10262.
- [51] D. Alesini et al., Phys. Rev. D **103**, 102004 (2021), 2012.09498.
- [52] C. M. Caves, Phys. Rev. D **26**, 1817 (1982), URL <https://link.aps.org/doi/10.1103/PhysRevD.26.1817>.
- [53] C. Macklin, K. O'Brien, D. Hover, M. E. Schwartz, V. Bolkhovskiy, X. Zhang, W. D. Oliver, and I. Siddiqi, Science **350**, 307 (2015), URL <http://www.sciencemag.org/content/350/6258/307.abstract>.
- [54] C. Eichler, J. Mlynek, J. Butscher, P. Kurpiers, K. Hammerer, T. Osborne, and A. Wallraff, Physical Review X **5** (2015), ISSN 2160-3308, URL <http://dx.doi.org/10.1103/PhysRevX.5.041044>.
- [55] M. P. da Silva, D. Bozyigit, A. Wallraff, and A. Blais, Phys. Rev. A **82**, 043804 (2010), URL <http://link.aps.org/doi/10.1103/PhysRevA.82.043804>.
- [56] K. M. Backes, D. A. Palken, S. A. Kenany, B. M. Brubaker, S. B. Cahn, A. Droster, G. C. Hilton, S. Ghosh, H. Jackson, S. K. Lamoreaux, et al., Nature **590**, 238–242 (2021), ISSN 1476-4687, URL <http://dx.doi.org/10.1038/s41586-021-03226-7>.
- [57] A. Pankratov, L. Revin, A. Gordeeva, A. Yablokov, L. Kuzmin, and E. Il'ichev, npj Quantum Inf **8**, 61 (2022).